[22] *G. Livescu, D. A. B. Miller, D. S. Chemla, M. Ramaswamy, T. Y. Chang, N. Sauer, A. C. Gossard,* and *J. H. English,* IEEE J. Quant. Electron. **24** (1988) 1677.
[23] *D. Huang, H. Y. Chu, Y. C. Chang,* and *H. Morkoc,* Phys. Rev. **B38** (1988) 1246.
[24] *J. S. Lee, N. Miura,* and *T. Ando,* J. Phys. Soc. Jap. **59** (1990) 2254.
[25] *J. Wagner, A. Fischer,* and *K. Ploog,* Appl. Phys. Lett. **59** (1991) 428.
[26] *R. Cingolani, W. Stolz,* and *K. Ploog,* Phys. Rev. **B40** (1989) 2950.
[27] (a) *M. S. Skolnick, J. M. Rorison, K. J. Nash, D. J. Mowbray, P. R. Tapster, S. J. Bass,* and *A. D. Pitt,* Phys. Rev. Lett. **58** (1987) 2130; (b) *M. S. Skolnick, D. M. Whittaker, P. E. Simmonds, T. A. Fisher, M. K. Saker, J. M. Rorison, R. S. Smith, P. B. Kirby,* and *C. R. H. White,* Phys. Rev. **B43** (1991) 7354.
[28] *W. Chen, M. Fritze, A. V. Nurmikko, D. Ackley, C. Colvard,* and *H. Lee,* Phys. Rev. Lett. **64** (1990) 2434.
[29] *J. Wagner, A. Ruiz,* and *K. Ploog,* Phys. Rev. **B43** (1991) 12134.
[30] *A. E. Ruckenstein* and *S. Schmitt-Rink,* Phys. Rev. **B35** (1987) 7551.
[31] *S. Schmitt-Rink, D. S. Chemla,* and *D. A. B. Miller,* Adv. in Phys. **38** (1989) 89.
[32] *K. Ohtaka* and *Y. Tanabe,* Phys. Rev. **B39** (1989) 3054.
[33] *T. Uenoyama* and *L. J. Sham,* Phys. Rev. Lett. **65** (1990) 1048.
[34] *G. E. W. Bauer,* in: Localization and Confinement in Semiconductors, ed. by *G. Bauer, F. Kuchar,* and *H. Heinrich,* 6th International Winterschool, Mauterndorf, February 1990. Springer-Verlag, Berlin, in press.
[35] *I. E. Perakis* and *Y. C. Chang,* Phys. Rev. **B43** (1991) 12556.
[36] *J. F. Müller, A. E. Ruckenstein,* and *S. Schmitt-Rink,* Mod. Phys. Lett. **B,** in press; *J. F. Müller,* Phys. Rev. **B42** (1990) 1189.
[37] *P. Hawrylak,* to appear in Sol. State Comm. (1992).
[38] *L. Brey, N. Johnson,* and *B. I. Halperin,* Phys. Rev. **B40** (1989) 10647; *P. A. Maksym* and *T. Chakraborty,* Phys. Rev. Lett. **65** (1990) 108; *Q. P. Li* et al., Phys. Rev. **B43** (1991) 5151.
[39] *S. E. Laux, D. J. Frank,* and *F. Stern,* Surf. Sci. **196** (1988) 101.
[40] *Q. P. Li* and *S. Das Sarma,* Phys. Rev. **B43** (1991) 11768.
[41] *J. Gavoret, P. Nozières, B. Roulet,* and *M. Combescot,* J. Phys. (Paris) **30** (1969) 987.

Reprinted from Optics of Semiconductor Nanostructures, F. Henneberger, S. Schmidtt-Rink and E. O. Gobel, Editors (Akademie Verlag, Berlin, 1993) p. 361-395.

III.3
Size Scaling and Exciton Coherence-Size in the Optical Non-linearities of Conjugated Polyenes

S. Mukamel and *H. X. Wang*

Abstract

The elementary excitations of conjugated polyenes are calculated using a quasi-particle approach. We show that the electron and the hole created optically remain in close proximity and form charge-transfer excitons. The size-scaling and saturation of $\chi^{(3)}$ are shown to result from quantum confinement of the relative electron-hole excitonic motion.

III.3.1 Introduction

Organic compounds with conjugated π- or σ-electrons may have remarkably large nonlinear optical (NLO) response and are therefore drawing a considerable experimental and theoretical attention [1–4]. The electrons in conjugated molecules are divided into two groups. The σ-electrons which occupy an sp^2 hybrid orbital, form the molecular backbone and are localized. The π-electrons occupy the $2p_z$ atomic orbitals, and due to their strong overlap, they are delocalized. It is the mobility and the delocalization of the π-electrons that are responsible for the unusually large optical response of conjugated molecules.

One of the most fascinating challenges of the theoretical modelling of conjugated polymers is that they can be approached from two opposite ends: from a molecular [4–11] or a semiconductor [12, 13] viewpoint. In the molecular picture, optical nonlinearities require the calculation of the

exact molecular (many-electron) eigenstates and dipole matrix elements. Recent calculations of $\chi^{(3)}$ and its frequency dispersion in small conjugated polyenes show a remarkable agreement with two-photon absorption, third harmonic generation, and nonlinear refractive index measurements [5, 14–16]. Such calculations are limited to small polyenes or the Hückel model [17] since both the calculation of molecular eigenstates and the multiple summations involved in the susceptibilities are quite tedious, particularly for off-resonant response which requires a sum over many eigenstates. On the other hand, adopting the semiconductor viewpoint, we directly consider elementary excitations (electron-hole pairs) using many-body Green function techniques. This approach [18, 19] provides a transparent physical picture of the nonlinear optical process, and offers a direct means for incorporating Coulomb interactions as well as exciton formation and coupling with phonons. It also provides a unified description of conjugated polyenes and artificially fabricated semiconductor nanostructures [20].

Much effort is being devoted to manipulating the magnitude of the off-resonant nonlinear response and investigating its scaling with size, which are crucial for the practical applications of optical materials [6–10, 21]. A strong nonlinear size scaling was first measured using third harmonic generation for the range of $N=3-19$ by *Hermann* and *Ducuing* [21], N being the number of the double bonds. A power scaling law on molecular size $\chi^{(3)}\sim N^b$ has been proposed by many authors [6–10, 21, 22]. *Rustagi* and *Ducuing* have used a free electron model where the polyene is modelled as a noninteracting electron gas in a one dimensional box. They derived the following expression for $\chi^{(3)}(0)$ for large N:

$$\chi^{(3)}(0)=256d_0^5N^5/(45a_0^3q^2\pi^6). \tag{1}$$

Where $a_0\equiv\hbar^2/m_eq^2$ is the atomic Bohr radius (m_e is the electron mass), d_0 is the sum of double and single bond lengths, and q is the electron charge. This expression corresponds to a power law with scaling exponent $b=5$. Estimates of the scaling exponent b vary from 6 to 3.5 for the size range ($N=2-12$). The scaling with size using the Hückel model was discussed in terms of the alternate coupling constants $\beta(1-\delta)$ and $\beta(1+\delta)$. *McIntyre* and *Hameka* [9] obtained $b=5.257$ for $N=3-11$ for the Hückel model with no alternation ($\delta=0$) using a double-perturbation treatment of the ground state energy. *Flytzanis* and coworkers [22] defined a coherence length in terms of the band gap and the alternate coupling constant as

$N_d\equiv1/\delta$. For $\delta=0$, using the Hückel model and a variational perturbative method, they recovered the same results of *Ducuing's* free electron in a box model (Eq. (1)). Then for $\delta\neq0$ using a sum over states approach, they found

$$\chi^{(3)}(0)=8/21(q^4/|k_F|^4E_F^3)(2E_F/E_g)^6, \tag{2}$$

where k_F and $E_F\equiv2\beta$ which do not depend on δ are the Fermi wavevector and energy respectively, and $E_g=4\delta\beta$ is the band gap energy. Eq. (2) predicts $\chi^{(3)}\sim\delta^{-6}$ and an infinite $\chi^{(3)}$ when $\delta=0$, which contradicts the calculations of *McIntyre* and *Hameka,* who predict a finite $\chi^{(3)}$ in this limit. Recently, values of $b=4.32$ [10a] for the range of $N=2-10$ were reported by *Shuai* and *Brédas* using the Hückel (single electron) model. Similar values were found when Coulomb interactions are incorporated by *Garito* and coworkers [6] who used the Pariser-Parr-Pople (PPP) model and the complete neglect of differential overlap/spectroscopic (CNDO/S) approximation. Both the singly and the doubly excitation configurations were included by using the self-consistent-field (SCF) molecular-orbital (MO) method with configuration interactions (CI). These calculations resulted in $b=4.6$ for the size range $N=2-8$. *DeMelo* and *Silbey* obtained $b=5.27$ for $N=2-10$ [7], using a variation-perturbation treatment of the density matrix and the PPP hamiltonian.

Physically, we expect the sharp nonlinear scaling with size to hold only in a limited size range and to saturate for large N where the thermodynamic limit implies that $b=1$. Such saturation has been predicted by *Beratan* et al. [10b] around $N=40$ using Hückel model including only single particle excitation configurations. *Brédas* and *Shuai* have used the Hückel model with a sum over states approach and partially including two-particle excitations. They obtained a saturation size of $N=50$ [10a].

Exploring the origin of the nonlinear response, and the factors determining the magnitude and the response timescale of large polyenes and their scaling and saturation with size, constitutes an important experimental and theoretical challenge. A major obstacle in the theoretical modelling of these phenomena is the lack of an efficient method for computing the nonlinear response, particularly for large polyenes when Coulomb interactions are included, where the conventional sum over molecular eigenstates expressions become prohibitively tedious.

In this chapter we present an anharmonic-oscillator picture for the nonlinear optical response of conjugated polymers, developed using equations

of motion for two-particle (electron-hole) variables [19]. The method allows a very efficient calculation of the nonlinear response over a broad range of sizes and Coulomb interactions, and resolves the ambiguity regarding the scaling exponent. We clearly identify the elementary excitations as *charge-transfer-excitons* which are intermediate between the molecular (Frenkel) and the semiconductor (Wannier) excitons [12]. The coherence-length determining the scaling and the saturation of $\chi^{(3)}$ with size is shown to be related to the exciton size associated with the relative electron-hole motion. The present theory highlights the close similarity of polyenes and semiconductor quantum dots and quantum wires [20], which show the same trends such as the blue shift with decreasing size (quantum exciton confinement) and the interplay of the coherence sizes associated with the relative and the translational motions of the electron-hole pair [23]. The remainder of this chapter is divided into five sections. In Sec. III.3.2 we present the model hamiltonian in the Wannier representation. In Sec. III.3.3 we derive the equations of motion which map the calculation onto the dynamics of anharmonic nonlocal exciton oscillators. In Sec. III.3.4, we present a Green function expression for $\chi^{(3)}$ using the PPP model. In Sec. III.3.5 we present numerical calculations for the off-resonant $\chi^{(3)}(0)$ and the time evolution of excitons. Finally in Sec. III.3.6 we summarize our results.

III.3.2 Wannier Representation of the PPP Hamiltonian

Our study is based on the Pariser-Parr-Pople (PPP) hamiltonian which consists of the tight-binding single-electron (SSH or Hückel) hamiltonian with the addition of Coulomb interactions [4]. The Hückel model represents a linear chain with N double bonds and a single $2p_z$ orbital per site, and with alternating exchange couplings $\beta(1-\delta)$, $\beta(1+\delta)$,

$$H_0 = \sum_{n=1}^{H} |2n\rangle\, \beta(1-\delta)\, \langle 2n+1| + |2n\rangle\, \beta(1+\delta)\, \langle 2n-1|. \tag{3}$$

Here $|n\rangle$ represent an electron in the $2p_z$ orbital at the nth carbon atom. The Coulomb interaction between two electrons located at positions x and x' is modeled using the Ohno formula,

$$Z(x-x') = U[1+((x-x')/q^2U)^2]^{-1/2}, \tag{4}$$

q being the electron charge and U is the on-site Hubbard interaction energy. Instead of attempting to solve for the molecular eigenstates, we now recast this hamiltonian in an electron-hole language which will allow us to develop a quasiparticle picture for the optical nonlinearities, and connect it with semiconductor nanostructures. To that end we first calculate the eigenvalues $H_0\Phi = E\Phi$ of the Hückel model using periodic boundary conditions $\Phi_{vk}(N+1) = \Phi_{vk}(1)$. The N lower (higher) eigenstates Φ_{vk} (Φ_{ck}) constitute the valence (conduction) band, with energies ε_{vk} (ε_{ck}), respectively [19, 24]. Using these band functions, we then construct a new basis set of *Wannier functions*,

$$W_{v,n}(x) = \frac{1}{\sqrt{N}} \sum_k e^{ikn} \Phi_{vk}(x). \tag{5}$$

The Wannier functions at different sites form an orthonormal basis of localized electronic states, where $W_{v,n}$ is localized on the nth double bond. We next introduce creation and annihilation operators corresponding to the Wannier basis. $c_n^\dagger$ creates an electron in the $W_{c,n}(x)$ state, and $d_n^\dagger$ creates a hole in the $W_{v,n}(x)$ state. The corresponding annihilation operators are c_n and d_n. These operators satisfy the Fermi commutation rules, $[c_n, c_m^\dagger] = \delta_{nm} - 2c_m^\dagger c_n$, $[d_n, d_m^\dagger] = \delta_{nm} - 2d_m^\dagger d_n$, and all other commutators $[c_n, d_m^\dagger]$ etc. vanish.

The total PPP hamiltonian recast in the electron-hole representation is then given by

$$H = H_0 + H' + H_{\text{int}}, \tag{6}$$

$$H_0 = \sum_{nm} [c_n^\dagger c_m H_{nm}^c - d_m^\dagger d_n H_{nm}^v]. \tag{7}$$

H_{nm}^v with $v = c, v$ are the matrix elements of the Hückel hamiltonian in the Wannier basis,

$$\langle W_{v,n}|H_0|W_{v',m}\rangle \equiv H_{nm}^v \delta v v'. \tag{8}$$

Using Eq. (5), we get

$$H^{\nu}_{nm} = \pm \frac{\beta\sqrt{2}}{N} \sum_{k} e^{-ik(n-m)} \varepsilon_{\nu k}. \tag{9}$$

The + and the − signs in Eq. (9) and (8) stand for $\nu = c$ (conduction band) and $\nu = v$ (valence band), respectively. The Coulomb interaction H' reads:

$$H' = \sum_{nm} \left[\frac{1}{2} V_1(nm) \left(c^{\dagger}_n c^{\dagger}_m c_m c_n + d^{\dagger}_m d^{\dagger}_n d_n d_m - 2 c^{\dagger}_n c_n d^{\dagger}_m d_m\right) + V_2(nm) c^{\dagger}_m c_n d^{\dagger}_m d_n \right]. \tag{10}$$

$V_1(nm)$ is the Coulomb and $V_2(nm)$ is the exchange interaction between two charges in two Wannier states localized at the n and the m unit cells. These interactions may be expressed in terms of the matrix element,

$$V\binom{n_1 n_2 n_3 n_4}{\nu_1 \nu_2 \nu_3 \nu_4} \equiv \int\int W^{*}_{\nu_1, n_1}(x)\, W^{*}_{\nu_2, n_2}(x')\, Z(x-x')\, W^{*}_{\nu_3, n_3}(x')\, W^{*}_{\nu_4, n_4}(x)\, dx'\, dx, \tag{11}$$

where $\nu_j = c, v$ is the band index, and n_j denote the position of the Wannier function along the chain. When the overlap of the Wannier functions is neglected, Eq. (11) vanishes unles $n_1 = n_2$, and $n_3 = n_4$, and we get

$$V_1(nm) = V\binom{nmmn}{vvvv} = V\binom{nmmn}{cvvc} = V\binom{nmmn}{vccv} = V\binom{nmmn}{cccc}, \tag{12}$$

$$V_2(nm) = V\binom{nmmn}{cvcv} = V\binom{nmmn}{vcvc}. \tag{13}$$

The Coulomb interaction $V_1(nm)$ affects the relative motion of the electron-hole pair, and may create bound (exciton) states. As a result of the exchange interaction $V_2(nm)$, the excited states may become delocalized even in molecular crystals where the electrons are localized.

H_{int} denotes the interaction hamiltonian between the molecule and the external electric field $E(r, t)$,

$$H_{\text{int}} = -\sum_{nm} P_{nm}\, E((n+m/2), t). \tag{14}$$

Here P_{nm} is a nonlocal contribution to the polarization operator representing a coherence between the n and m bonds,

$$P_{nm} \equiv \mu^{c}_{nm} c^{\dagger}_n c_m - \mu^{v}_{nm} d^{\dagger}_m d_n + \mu^{vc}_{nm} c^{\dagger}_n d^{\dagger}_m + \mu^{cv}_{nm} d_m c_n, \tag{15}$$

$E((n+m)/2, t)$ is the electric field at the average position of these two bonds. μ^{cv}_{nm} is the interband transition dipole,

$$\mu^{cv}_{nm} \equiv q \int W^{*}_{c,n}(x)\, x\, W_{v,m}(x)\, dx, \tag{16}$$

whereas μ^{c}_{nm} and μ^{v}_{nm} are the intraband transition dipoles,

$$\mu^{c}_{nm} = \mu^{v}_{nm} \equiv q \int W^{*}_{c,n}(x)\, x\, W_{c,m}(x)\, dx. \tag{17}$$

Since the hamiltonian does not depend on spin, the electron and the hole created by the dipolar interaction with the external fields must carry an opposite spin (i.e. they form a singlet exciton). For clarity we have therefore omitted the spin label in the present notation. Using translational symmetry, it follows that $V_1(nm)$, $V_2(nm)$, μ^{c}_{nm}, μ^{cv}_{nm} depend only on the separation $n-m$ of the two bonds. All quantities appearing in the hamiltonian can be expressed in terms of the four basic parameters of the PPP hamiltonian: β, δ, q, and U [19].

III.3.3 Equations of Motion in the Electron-Hole Anharmonic Oscillator Representation

In the ground (vacuum) state of the Hückel model, all of the N valence-band states are occupied by two electrons. Upon optical excitation, an electron may move from the ground state to any of the unoccupied states in the conduction band, creating a hole in the valence band. The lowest transition energy will be from the top of the valence band to the bottom

of the conduction band. This picture changes once Coulomb interaction between the electron and the hole is incorporated in the PPP hamiltonian. The electron at site n and the hole at site m may form a bound exciton due to their attractive Coulomb interaction. The excitons undergo two types of motion, related to their translational motion along the molecular chain, and the relative motion of the pair. The separate treatment of these motions is best accomplished by introducing the binary variable coordinates as follows,

$$Y_{s,k} \equiv \frac{1}{\sqrt{N}} \sum_{r=1}^{N} e^{-ikr} d_{r+s/2} c_{r-s/2}, \tag{18a}$$

$$Y^{\dagger}_{s,k} \equiv \frac{1}{\sqrt{N}} \sum_{r=1}^{N} e^{ikr} c^{\dagger}_{r-s/2} d^{\dagger}_{r+s/2}. \tag{18b}$$

Here r and s represent the translational and the relative coordinates, respectively. To exploit the translational symmetry of the problem, we treat the translational motion in momentum (k) space. Similarly we define additional binary operators representing electron-coherence and hole-coherence:

$$C_{s,k} \equiv \frac{1}{\sqrt{N}} \sum_{r=1}^{N} e^{-ikr} c^{\dagger}_{r-s/2} c_{r+s/2}, \tag{19a}$$

$$D_{s,k} \equiv \frac{1}{\sqrt{N}} \sum_{r=1}^{N} e^{-ikr} d^{\dagger}_{r-s/2} d_{r+s/2}. \tag{19b}$$

We shall be interested in the third-order frequency-domain response to an applied electric field. Hereafter we assume a homogeneous excitation, i.e. the field does not depend on position, $E(r, t) = E(t)$. This holds when the field is polarized along the chain, or when the polyene size is much smaller than the optical wavelength. The radiation-matter interaction is then given by

$$H_{\text{int}} = -P\,E(t). \tag{20}$$

Here the total polarization operator is given by

$$P = \sum_{s,k} [\mu_s (Y_{s,k} + Y^{\dagger}_{s,k}) + \mu^{c}_{s,k} (C_{s,k} + D_{s,k})], \tag{21}$$

and we have defined

$$\mu_s \equiv \mu^{cv}_s = \mu^{vc}_s \equiv \frac{1}{\sqrt{N}} \sum_{r}^{N} e^{-ikr} \mu^{cv}_{r+s/2,r-s/2}, \tag{22a}$$

$$\mu^{c}_{s,k} = \mu^{v}_{s,k} \equiv \frac{1}{\sqrt{N}} \sum_{r}^{N} e^{-ikr} \mu^{c}_{r+s/2,r-s/2} \equiv \mu'_s \delta_{k,0} + g_k \delta_{s,0}. \tag{22b}$$

Using the Heisenberg equation $\dot{A} = i/\hbar [H, A]$ together with the hamiltonian (Eq. (6)), we have derived equations of motions for the $Y_{s,k}$, $C_{s,k}$ and $D_{s,k}$ operators (eqs. (A1)). Once expectation values are taken, the resulting equations are not closed. They contain in the r.h.s. new higher-order dynamical variables, namely $\langle C_{s',k'} Y_{s,k} \rangle$ and $\langle D_{s',k'} Y_{s,k} \rangle$. A rigorous way to proceed is to use the Heisenberg equation again to derive more equations for these new variables. This procedure will eventually generate an infinite hierarchy of equations. We have closed the hierarchy by taking expectation values of Eqs. (A1) and then making the factorizations:

$$\langle C_{s',k'} Y_{s,k} \rangle = \langle C_{s',k'} \rangle \langle Y_{s,k} \rangle, \tag{23}$$

$$\langle D_{s',k'} Y_{s,k} \rangle = \langle D_{s',k'} \rangle \langle Y_{s,k} \rangle. \tag{24}$$

Solving these equations perturbatively in the radiation field results in the optical susceptibilities. To that end we expand the expectation values of all operators in powers of the external field, and solve for $\langle Y_{s,k} \rangle$, $\langle C_{s,k} \rangle$ and $\langle D_{s,k} \rangle$, and the polarization order by order. The resulting equations expanded to third order in the field are given in the appendix. These equations thus map the calculation onto the dynamics of $N(2N-1)$ coupled anharmonic oscillators. (N^2, $N(N-1)/2$ and $N(N-1)/2$ non-local oscillators representing the electron-hole pair ($\langle Y_{s,k} \rangle$), electron-coherence ($\langle C_{s,k} \rangle$) and hole-coherence ($\langle D_{s,k} \rangle$) respectively.) Anharmonic-oscillator modeling of optical nonlinearities has been suggested as a qualitative model since the early days of nonlinear optics [25], and the picture has been firmly established recently for Frenkel excitons in molecular nanostructures with localized electronic states [26]. The present calculation extends these ideas to conjugated polyenes. The following calculations were performed in the frequency domain, where the optical polarization is

given by

$$\langle P(\omega)\rangle=\sum_{s,k}\left[\mu_s(\langle Y_{s,k}(\omega)\rangle+\langle Y^{\dagger}_{s,k}(\omega)\rangle)+\mu^{c}_{s,k}(\langle C_{s,k}(\omega)\rangle+\langle D_{s,k}(\omega)\rangle)\right], \quad (25)$$

and we adopt the following definition of a Fourier transform,

$$A(\omega)=\frac{1}{\sqrt{2\pi}}\int_{-\infty}^{\infty} dt e^{-i\omega t}A(t), \quad (26)$$

where $A=Y_{s,k}$, $C_{s,k}$ and $D_{s,k}$.

III.3.4 Green Function Expression for $\chi^{(3)}$

The solution of the equations of motion, and the optical response, may most conveniently be expressed in terms of Green functions representing the electron and hole motions. These Green functions are introduced below.

The Green function $G_{s,s'}(k, t)$ describes the motion of a single electron-hole pair. It is defined by setting $C_{s,k}=D_{s,k}=0$ and $E(t)=0$ in Eqs. (A1), and solving for $Y_{s,k}(t)$, i.e.,

$$\dot{Y}_{s,k}(t)=\sum_{s'} G_{s,s'}(k, t)\, Y_{s',k}(t=0). \quad (27)$$

The Green function in the frequency-domain is given by

$$G^{-1}_{s,s'}(k, \omega)\equiv\omega^{c}_{s'-s}e^{-ik(s'-s)/2}-\omega^{v}_{s'-s}e^{ik(s'-s)/2} + V_2(s)\delta_{s',-s}-(V_1(s)+\omega)\delta_{s',s}. \quad (28)$$

The motion of a single electron in the conduction band is described by the $F_{s,s'}(k, \omega)$ Green function. Setting $Y_{s,k}=C_{s,k}=0$ and $E(t)=0$ in Eqs. (A1) we obtain the solution

$$\dot{C}_{s,k}(t)=\sum_{s'} F_{s,s'}(k, t)\, C_{s',k}(t=0), \quad (29)$$

which in the frequency-domain gives

$$F^{-1}_{s,s'}(k, \omega)\equiv 2\omega^{c}_{s'-s}\sin[k(s'-s)/2] -(V_1(s)-V_1(0)+\omega)\delta_{s',s}+\sum_{s''}\left[V_1(s'')\delta_{s',0}-V_1(s'')\delta_{s',s}\right]. \quad (30)$$

Finally, the motion of a single hole in the valence band is described by the $Q_{s,s'}(k, \omega)$ Green function. Setting $Y_{s,k}=C_{s,k}=0$ and $E(t)=0$ in Eqs. (A1) we obtain the solution

$$\dot{D}_{s,k}(t)=\sum_{s'} Q_{s,s'}(k, t)\, D_{s,k}(t=0), \quad (31)$$

and in the frequency domain we get

$$Q^{-1}_{s,s'}(k, \omega)\equiv 2\omega^{v}_{s'-s}\sin[k(s'-s)/2] -[V_1(s)-V_1(0)+\omega]\delta_{s',s}+\sum_{s''}\left[V_1(s'')\delta_{s',0}-V_1(s'')\delta_{s',s}\right]. \quad (32)$$

Hereafter we shall also use these Green functions at $k=0$. We therefore further introduce the abbreviated notations, $G_{s,s'}(\omega)\equiv G_{s,s'}(k=0, \omega)$, $F_{s,s'}(\omega)\equiv F_{s,s'}(k=0, \omega)=Q_{s,s'}(k=0, \omega)$. The physical significance of these Green functions is as follows: $G_{s,s'}(k, \omega)$ describe the translational and the relative motions of an electron-hole pair. By taking $k=0$, we assume a homogeneous excitation of the pair, and the translational degree of freedom drops out of the problem, $G_{s,s'}(\omega)$ thus represents only the relative motion. $F_{s,s'}(\omega)$ describe the momentum dynamics of a uniformly prepared electron (using the Wigner representation, the electron momentum is the conjugate variable to s) [13, 27]. Similarly $Q_{s,s'}(\omega)$ describes the momentum dynamics of a uniformly prepared hole.

Using these Green functions, we have derived closed form expressions for the optical susceptibilities. For the linear response we get

$$\chi^{(1)}(\omega)=\varrho[\alpha(\omega)+\alpha(-\omega)], \quad (33)$$

with

$$\alpha(\omega)=\sum_{s,s'}\mu_s\mu_{s'}G_{s,s'}(\omega), \quad (34)$$

ϱ being the molecular number density. We next consider the third-order susceptibility. For a general four wave mixing process with three incoming fields ω_1, ω_2 and ω_3, generating a polarization at $\omega_f \equiv \omega_1 + \omega_2 + \omega_3$, we have

$$\chi^{(3)}(-\omega_f; \omega_1, \omega_2, \omega_3) = \varrho \sum_p [\gamma(\omega_1, \omega_2, \omega_3) + \gamma(-\omega_1, -\omega_2, -\omega_3)], \quad (35)$$

with

$$\begin{aligned}
\gamma(\omega_1, \omega_2, \omega_3) &= 2 \sum_{ss's_1s_2s_3s_4} \mu_s \mu_{s_4} \mu_{s_1+s'} \mu_{s_3-s_2} \\
&\times G_{s,s'}(\omega_f)\, F_{s_1,s_2}(\omega_1+\omega_2)\, G_{s_3,s_4}(\omega_1) \\
&+ \frac{4}{\sqrt{N}} \sum_{ss's_1s_2s_3kk'} \sin(k(s_3 - s'/2)) \sin(k' s_1/2)\, \mu_s \mu_{s_2} \mu^c_{s_3-s',k} \mu^c_{s_2,k'} \\
&\times G_{s,s'}(k, \omega_f)\, G_{s_3,s_1}(k', \omega_1+\omega_2)\, G_{s_1,s_2}(\omega_1) \\
&- \frac{2}{\sqrt{N}} \sum_{s's_1s_2s_3k} \sin(k s_1/2)\, \mu_{s_3+s'} \mu_{s_2} \mu^c_{s,k} \mu^c_{s_2,k} \\
&\times [F_{0,-s'}(k, \omega_f) - Q_{0,s'}(k, \omega_f)]\, [G_{s_3,s_1}(k, \omega_1+\omega_2) + F_{s_1,s'}(\omega_1+\omega_2)] \\
&\times G_{s_1,s_2}(\omega_1) + \sum_{ss's_1s_2s_3s_4s_5} V_2(s'-s_2)\, \mu_s \mu_{s_5} \mu_{s_1-s_4} \mu_{s_3} \\
&\times G_{s,s'}(\omega_f)\, [F_{s_2-s',s_1}(\omega_1+\omega_2) + F_{s_2-s',-s_1}(\omega_1+\omega_2)]\, G_{s_2,s_3}(\omega_1)\, G_{s_4,s_5}(\omega_2).
\end{aligned} \quad (36a)$$

The s summations run from 0 to $N-1$, and the k summations run from 1 to N. The p summation stands for the sum over all $3! = 6$ permutations of the three incoming frequencies ω_1, ω_2 and ω_3. All the terms in (36a) contain three Green function factors which, from right to left, describe the evolution of the system following the first, the second and the third interactions with the external electric field [28], respectively. The first term in $\chi^{(3)}$ (Eq. (36a)) represents the contributions of inter-band transitions alone, with the electron or hole Green functions $F_{s,s_1}(\omega)$ or $Q_{s,s_1}(\omega)$ describing the time evolution following the second interaction with the field. The second and third terms represent the combination of inter-band and intra-band transitions. They contain two inter-band transition dipoles μ_s and two intra-band transition dipoles $\mu^c_{s,k}$. In the second term, the system's evolution is described solely by the electron-hole Green functions $G_{s,s_1}(k, \omega)$ and $G_{s,s_1}(\omega)$. In the third term the system's evolution is described by the electron or the hole Green functions after the second interaction. The last term, which is proportional to the intersite Coulomb interaction, represents the local field interaction-induced contributions.

The present expression for $\chi^{(3)}$ which contains summations over oscillators is much more compact than the conventional expressions based on multiple summations over molecular eigenstates [25], and allows us to explore in depth the size scaling and saturation of the nonlinear response over a broad range of sizes. Interference effects between one-particle and two-particle excitations resulting in cancellation of large terms are naturally built into this picture and the cancellations are made prior to the calculation [26].

III.3.5 Calculations and Discussion

Off-resonant $\chi^{(3)}$

In the static limit, Eq. (36a) assumes the form

$$\begin{aligned}
\gamma(0,0,0) &= \frac{4}{\sqrt{N}} \sum_{ss's_1s_2s_3k} \sin(k(s_3 - s')/2)\, \mu_s \mu'_{s_3-s'} \mu^c_{s_3,k} \mu^c_{s_2,k} \\
&\times G_{s,s'}(k, 0)\, [F_{s_3,s_1}(k, 0) + Q_{s_3,s_1}(k, 0)]\, G_{s_1,s_2}(0) \\
&- \frac{2}{\sqrt{N}} \sum_{s's_1s_2s_3k} \sin(k s'/2)\, \mu_{s_1+s_2} \mu_{s_3} \mu_{s_2,k} \mu_{s,k} \\
&\times [F_{0,s'}(k, 0) + Q_{0,s'}(k, 0)]\, F_{s',-s_1}(k, 0)\, G_{s_2,s_3}(0).
\end{aligned} \quad (36b)$$

In all the calculations presented below we show the static (off-resonant) $\chi^{(3)}(0) \equiv 12\varrho\gamma(0,0,0)$ calculated using $\beta = 2.4$ eV [4]. We start by considering the Hückel model. In the expressions derived previously we used an approximate solution using cyclic boundary conditions

$$\Phi_{v,k}(N+1) = \Phi_{v,k}(1), \quad v = \mathrm{c}, \mathrm{v}$$

which lends itself more easily to analytical calculations. The correction due to the cyclic boundary conditions is expected to decrease with polyene size since boundary effects are less important for larger polyenes. The cyclic eigenstates provide, however, a good picture for all sizes.

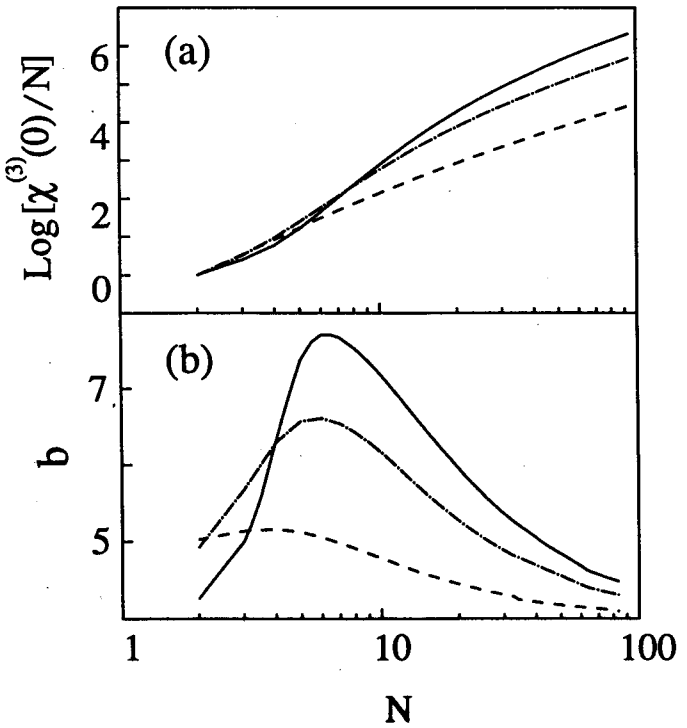

Fig. III.3.1 (a) Variation of the static $\chi^{(3)}$ per double-bond with size N using the anharmonic-oscillator picture in the Hückel model; solid: $\delta = 0.07$ (polyacetylene); dash-dot: $\delta = 0.15$ (polydiacetylene); dash: $\delta = 0.33$ (polysilane). (b) The scaling exponent $b = \mathrm{dlog}\,\chi^{(3)}(0)/\mathrm{dlog}\,N$, calculated using the slopes of the various curves of Fig. III.3.1a.

In Figs. III.3.1–III.3.3 we display $\chi^{(3)}$ calculated using the exact solution to the Hückel hamiltonian obtained by a numerical diagonalization of the $N \times N$ Hückel hamiltonian without incorporating any boundary conditions. In Fig. III.3.1a we display the variation of the static susceptibility $\chi^{(3)}(0)$ with δ. The values of δ shown 0.07, 0.15 and 0.33, correspond to polyacetylene, polydiacetylene, and polysilanes, respectively [4]. In Fig. III.3.1b we show the scaling exponent b which is related to the slopes of the curves displayed in Fig. III.3.1a ($b \equiv \mathrm{dlog}\,\chi^{(3)}(0)/\mathrm{dlog}\,(n)$). The exponent b reaches a maximum of $b = 7.7$ at $N = 6$ for $\delta = 0.07$, $b = 6.6$ at $N = 5$ for $\delta = 0.15$, and $b = 5.2$ at $N = 4$ for $\delta = 0.33$, and then drops to a value of ≈ 4 for $N \approx 100$. The "thermodynamic limit" should imply a saturation of these

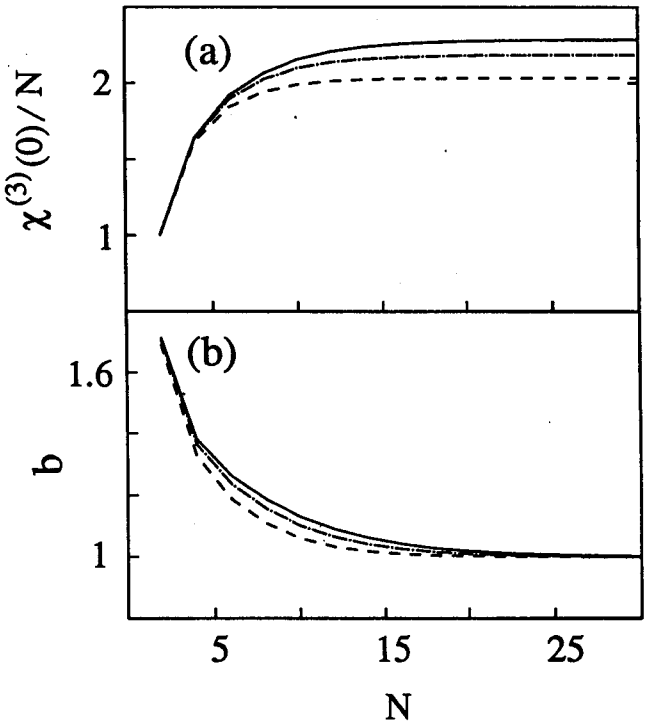

Fig. III.3.2 (a) Same calculation as in Fig. III.3.1 but with the neglect of the intraband transitions (i.e. setting $\mu^{v}_{s,k} = \mu^{c}_{s,k} = 0$. The enhancement with size is significantly reduced, illustrating the crucial role of intraband transitions in determining the magnitude of $\chi^{(3)}$. (b) The scaling exponent b for the various curves displayed in Fig. III.3.2a.

curves and $b=1$ ($\chi^{(3)}(0)/N$ independent on N for larger N). This limit is not achieved for the Hückel model in the size range considered here. Note that Hückel calculations usually use different parameters which reproduce the band gap without Coulomb interactions, whereas we are using here the PPP parameters with $U=0$. This may account for the discrepancy with recent calculations which showed a saturation at size $N=40-50$ [10].

In Fig. III.3.2 we repeat these calculations with the neglect of the intraband transitions, setting $\mu^{c}_{s,k}=\mu^{v}_{s,k}=0$. The enhancement with size is now considerably reduced, illustrating the crucial role of intraband transitions in determining the magnitude of $\chi^{(3)}$. This effect was found previously using the "essential state" picture based on the molecular eigenstates [5, 11].

In order to gain further insight into the significance of the present anharmonic-oscillator picture we have also considered the expression for $\chi^{(3)}$ using the sum over states approach, including the N^2 single-exciton and the $N^2(N-1)^2$ two-exciton states. We found some interesting interferences between the two-exciton and some of the single-exciton transitions which lead to a partial cancellation of terms. The oscillator picture builds naturally these interferences so that instead of calculating many terms and

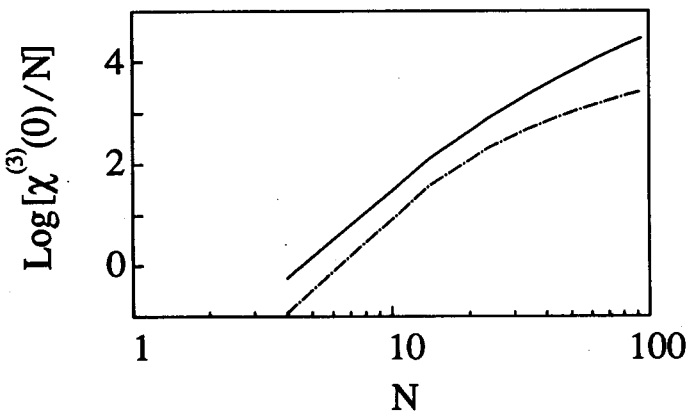

Fig. III.3.3 Solid line – variation of the total static $\chi^{(3)}$ per monomer with size, using the anharmonic-oscillator picture, for polydiacetylene $\delta=0.07$. Dash dot – the contribution of two-exciton (four particle) states to $\chi^{(3)}(0)$. This contribution was calculated using the sum-over-states expression (which is not given here). It is automatically included in the oscillator based expression (Eq. (36a)).

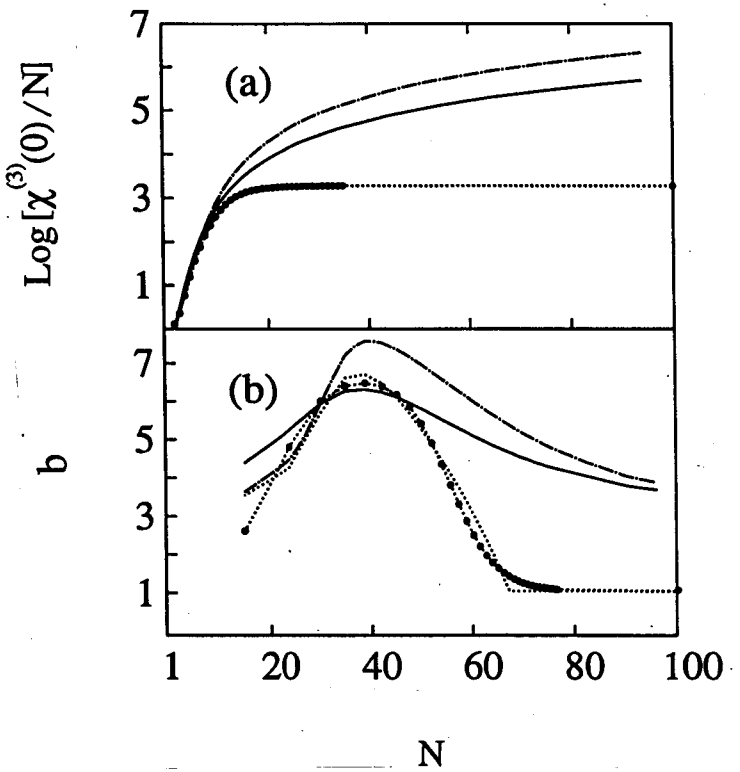

Fig. III.3.4 (a) Variation of static $\chi^{(3)}$ per double-bond for polyacetylene ($\delta=0.07$) with size N; solid: Hückel model; dashed-dot: Hückel model with cyclic boundary conditions; dotted: PPP model; circles: fit to the PPP calculation ($U=11.26$ eV). (b) slope of the curves in Fig. III.3.4a.

then canceling them, we get directly the more compact final outcome. A similar cancellation was found in nonconjugated nanostructures [26]. In Fig. III.3.3 we illustrate the relative contribution of two-exciton (four particle) states to $\chi^{(3)}(0)$. The solid line is the total $\chi^{(3)}(0)$ and the dash-dot curve represents only the contribution of terms which include two-exciton states. The figure shows that these later contributions are always smaller by a factor of at least 4 compared with the terms involving only single-exciton states.

In Fig. III.3.4, we present the variation of the static $\chi^{(3)}(0)$ with N for the PPP model. For comparison we also display the Hückel model

calculations; both the exact (solid line) solutions and the solutions with the cyclic boundary conditions (dashed-dot). The scaling of $\chi^{(3)}(0)$ in the PPP model with size was fitted with the following Pade expression (circles),

$$\chi^{(3)}(0) = [1 + (N/N_s')^5]/[1 + (N/N_s)^5], \tag{37}$$

where the saturation sizes are $N_s = 13.33$ and $N_s' = 2.94$. We note that for the PPP model $\chi^{(3)}(0)/N$ shows a rapid nonlinear dependence on size for small sizes, which saturates for larger sizes where the thermodynamics limit is obtained. The saturation is clearly seen by considering the slope b shown in the lower panel. The figure reveals some remarkable trends. We notice a sharp highly-nonlinear scaling with size for small sizes, which becomes more gradual for large sizes. The slope abruptly drops to $b = 1$ at a critical size $N_c = 21$. The nonanalytical behavior of the slope provides a natural definition for the nonlinear coherence size associated with $\chi^{(3)}(0)$ [19]. Note that the fit Eq. (37) does not reproduce the nonanalyticity and

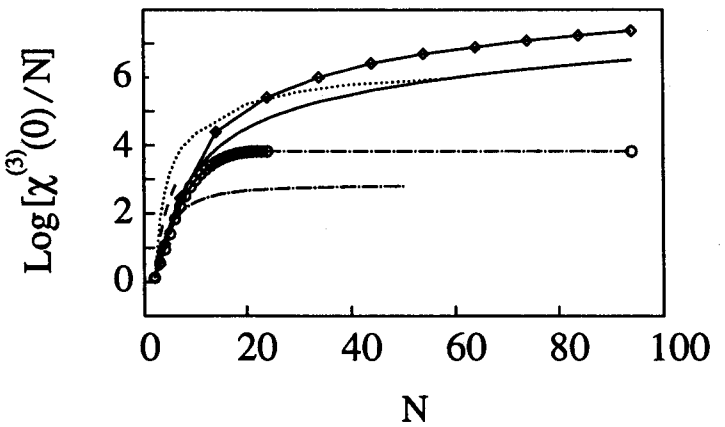

Fig. III.3.5 Variation of the static susceptibility $\chi^{(3)}(0)$ per double bond with polymer-size. Solid line: calculation using the anharmonic oscillator picture (Eq. (36a)), with numerical diagonalization of the SHH (Hückel) hamiltonian for polyacetylene ($\delta = 0.07$). Solid line with square: same calculation but with periodic boundary conditions. Dash-dot with circles: PPP model ($U = 11.26$ eV) and the fit (Eq. (37)). Other curves represent previous calculations. Dotted: *Beratan* et al. (Hückel model); dash-dotted: *Brédas* et al. (Hückel model); dashed: *Silbey* et al. (PPP model). The curves are normalized to the same value at $N = 2$. Solid line with circles present PPP results.

varies more smoothly across the critical value of N_c. The coherence size obtained here which corresponds 58 Å is in agreement with previous experimental and theoretical estimates. The coherence-size was predicted to be 25 Å by *Suhai* [29a], and estimated to be 33 Å by *Greene* et al. using photo-induced reflectivity measurements [29b]. A careful analysis of these results taking into account changes in the real part of the susceptibility [4a], and photo-induced transmission changes in thin films, lead to the modified estimate of the coherence size of 40 Å, as first shown in another PDA by *Etemad* and coworkers [30]. Using a sum over states approach where both the single- and double-configuration interactions were included, *Garito* and coworkers [6] predicted the coherence size to be 60 Å.

The different scaling of $\chi^{(3)}(0)$ for the Hückel and the PPP models can be rationalized as follows. As shown by studies of Frenkel excitons [18], the *translational* motion of the pair is expected to yield a scaling exponent of $b = 2$, at most. The sharp nonlinear scaling of $\chi^{(3)}$ must therefore be attributed to the formation of excitons and to the effect of restriction on the *relative* electron-hole motion (quantum size effects). That motion does not couple with the optical nonlinearity in the absence of Coulomb interactions (i.e. Hückel model). This argument is supported by the saturation of these curves as the Coulomb interaction is turned on. The saturation size decreases with the Coulomb interaction strength which determines also the bound exciton size. In Fig. III.3.5 we display the scaling of the third-order static susceptibility (Eq. (36a)) with molecular size for the size range of $N = 2$ to 94. The calculation compares very well with previous theories as shown in Fig. III.3.5. We reiterate that the present calculation is much simpler, since it only involves summations over oscillators. Since the periodic and the exact Hückel calculation yield very similar results for $\chi^{(3)}(0)$, we hereafter used the periodic boundary conditions in all the following figures.

Another spectroscopic observable that is sensitive to exciton confinement is the band gap E_g which increases as N decreases, resembling the blue shifts in semiconductor nanostructures [12, 20]. In Fig. III.3.6, we display the variation of the band gap E_g, $\log[\chi^{(3)}(0)/N]$, and κ_m which is a measure of exciton size (see discussion below) with molecular size N. The figure clearly shows that for large N, all three quantities saturate in a similar fashion.

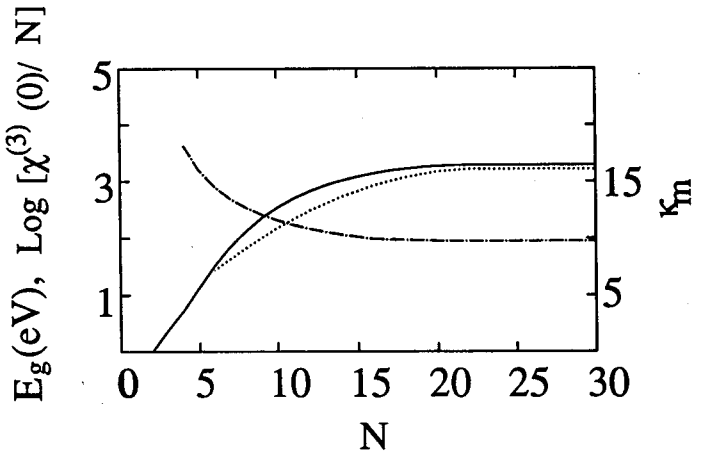

Fig. III.3.6 The variation with molecular size N of the band gap E_g (dashed-dot), the static $\log[\chi^{(3)}(0)/N]$ (solid line), and the participation ratio amplitude κ_m (dotted) for polyacetylene ($\delta = 0.07$).

Time Evolution of Charge-Transfer Excitons

The transition dipole μ_s controls the amplitude of creating an electron and a hole separated by s units. μ_s [19] is strongly localized, and for typical polyenes it has the largest values for $s=0$ and $s=1$ and then drops sharply. For polyacetylene, for example, $\mu_0 : \mu_1 : \mu_2 = 1 : .75 : 10^{-2}$ [19]. This suggests that the electron and the hole in conjugated polyenes are mainly created on the same site or on the nearest neighbor sites. The subsequent time evolution of the pair depends on the nature of the excitonic states of the system. In molecular assemblies [20] the electron and the hole are created on the same site ($s=0$) and remain so at all times. The tightly bound pair (known as Frenkel exciton) can undergo translational motion. In semiconductors, they form a more loosely bound pair (Wannier exciton) which resembles the hydrogen atom and spreads over many lattice sites. In charge-transfer crystals the situation is intermediate between these extremes; the electron and the hole are delocalized over a few sites [31, 32].

In order to explore the nature of the excitons in conjugated polyenes, and to find out whether they belong to any of the above categories, we

have calculated the time evolution of the pair following an impulsive (δ-function) excitation pulse at $t=0$. For simplicity we further assume that the polyene is small compared with the optical wavelength, so that the initial excitation is uniform ($k=0$). The initially prepared (unnormalized) doorway state is then

$$|\Phi(t=0)\rangle = P|0\rangle = \sum_s Y^{\dagger}_{s,0}|0\rangle. \tag{38}$$

The probability of the pair to be separated by s lattice units at time t is then given by

$$P_s(t) = |A_s(t)|^2 / \sum_s |\mu_s|^2, \tag{39}$$

where

$$A_s(t) \equiv \sum_{s'=0}^{N-1} G_{s,s'}(k, t)\mu_{s'}, \tag{40}$$

where $G_{s,s'}(k, t)$ is the Fourier transform of $G_{s,s'}(k, \omega)$, i.e.

$$G_{s,s'}(k, t) = \int e^{-i\omega t} G_{s,s'}(k, \omega)\, d\omega. \tag{41}$$

We can express this Green function in terms of the eigenstates $\Phi_\alpha(k, s)$ and the eigenvalues $E_\alpha(k)$ of the eigenvalue problem defined by Eq. (28), i.e.,

$$\sum_{s'} [\omega^{c}_{s'-s} e^{-ik(s'-s)/2} - \omega^{v}_{s'-s} e^{ik(s'-s)/2} + V_2(-s') - V_1(s')]\, \Phi_\alpha(k, s)$$
$$= E_\alpha(k)\, \Phi_\alpha(k, s). \tag{42}$$

We then have

$$G_{s,s'}(k, t) \equiv \sum_{\alpha=1}^{N} \Phi_\alpha(k, s)\, \Phi^*_\alpha(k, s) e^{-iE_\alpha(k)t}. \tag{43}$$

Eqs. (39) to (43) were used in the calculations presented in Figs. III.3.7 to III.3.12. In Fig. III.3.7 we display $P_s(t)$ for the Hückel model. In panels (a) and (b), we show the probability of finding the electron-hole pair at the

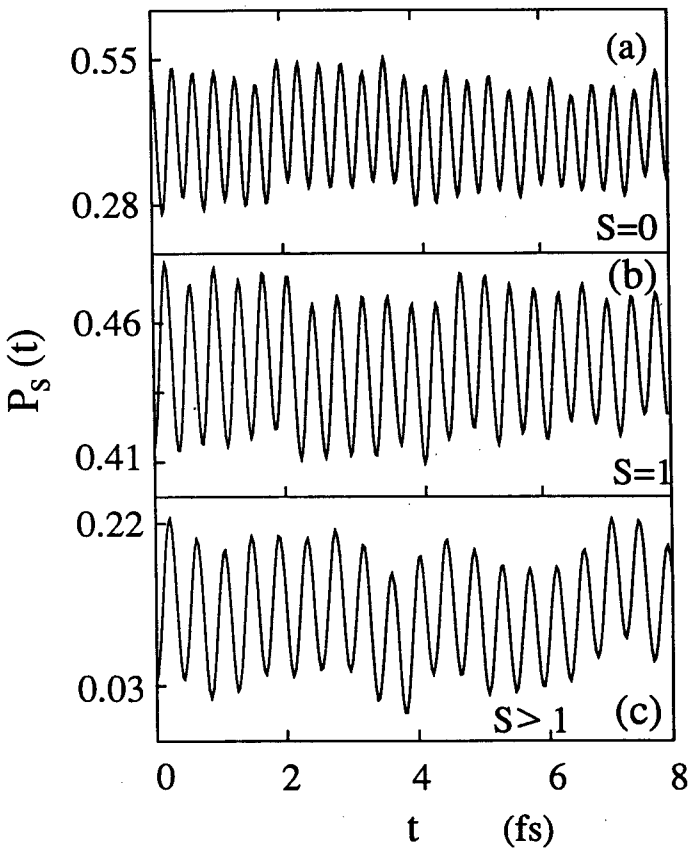

Fig. III.3.7 Exciton Motion in Hückel model. The probability $P_s(t)$ of finding exciton with electron-hole separation s after time t of the molecular-field interaction for polyacetylene ($\beta = 2.4$ eV, $\delta = 0.07$) with $N = 30$. (a) $P_0(t)$, (b) $P_1(t)$, (c) $1 - P_0(t) - P_1(t)$.

same site P_0 and at neighboring sites P_1. In panel (c), we show the probability of finding the electron-hole pair at all other sites $1 - P_0(t) - P_1(t)$. In Fig. III.3.8, we repeat these calculations for the PPP hamiltonian. Fig. III.3.7 shows that in the absence of Coulomb interactions, the electron-hole pair can move far apart. This picture changes for the PPP model as demonstrated in Fig. III.3.8. The Coulomb interaction binds the electron and the hole together and they can only be separated by essentially one bond; the probability of a large relative separation decreases dramatically.

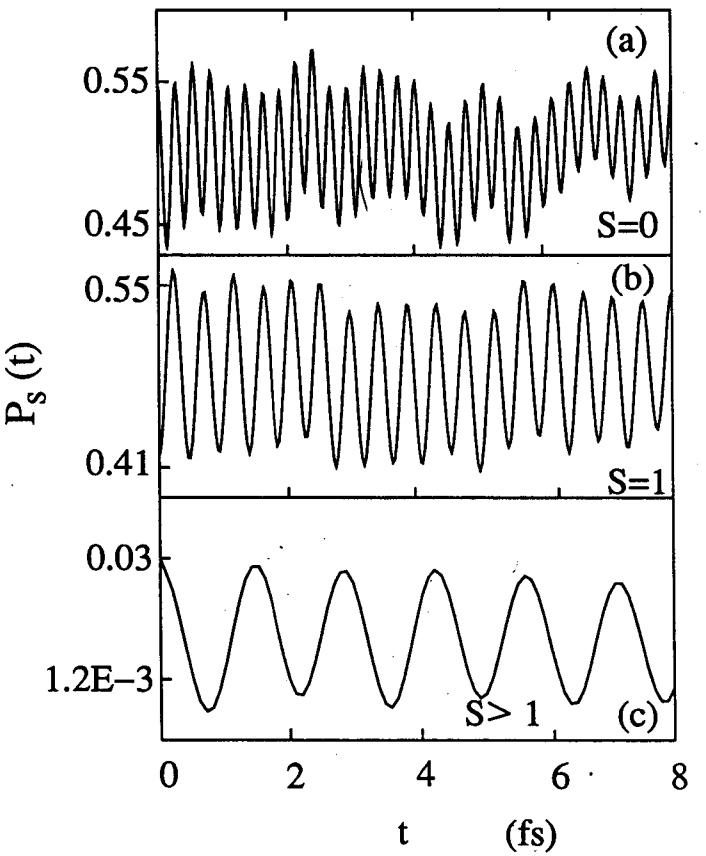

Fig. III.3.8 Exciton Motion in PPP model with $U = 11.26$ eV. The probability $P_s(t)$ of finding exciton with electron-hole separation s after time t of the molecular-field interaction for polyacetylene ($\delta = 0.07$) with $N = 30$. (a) $P_0(t)$, (b) $P_1(t)$, (c) $1 - P_0(t) - P_1(t)$.

A useful measure of the degree of delocalization of the pair is the *inverse participation ratio* [23, 33],

$$\kappa(t) \equiv 1/\sum_s P_s^2(t). \tag{44}$$

If the pair is separated over M sites then $P_s(t) \sim M^{-1}$ and therefore $\kappa \sim M$. In Fig. III.3.9 we plot $\kappa(t)$ for different values of the Coulomb interaction ranging from $U = 0$ (Hückel model) to $= 11.26$ eV for polyacetylene with

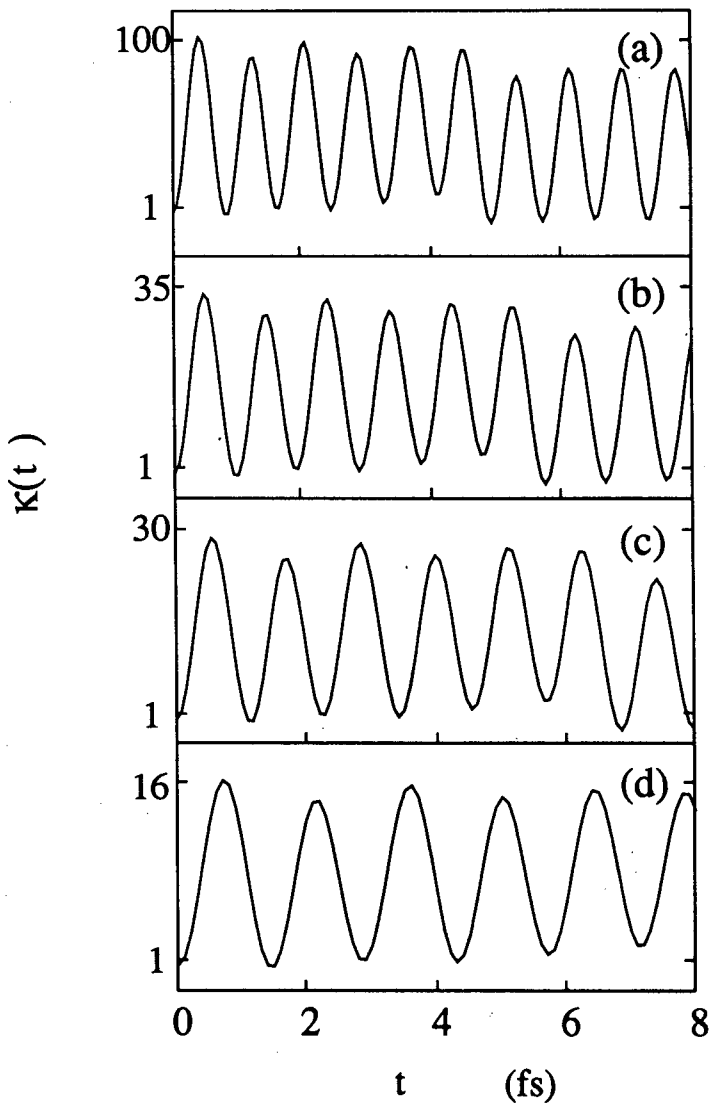

Fig. III.3.9 The inverse participation number $\kappa(t)$ for polyacetylene ($\delta = 0.07$) and different values of the Hubbard interaction magnitude U. (a) $U = 0$ eV, (b) $U = 4$ eV, (c) 8 eV, (d) $U = 11.26$ eV.

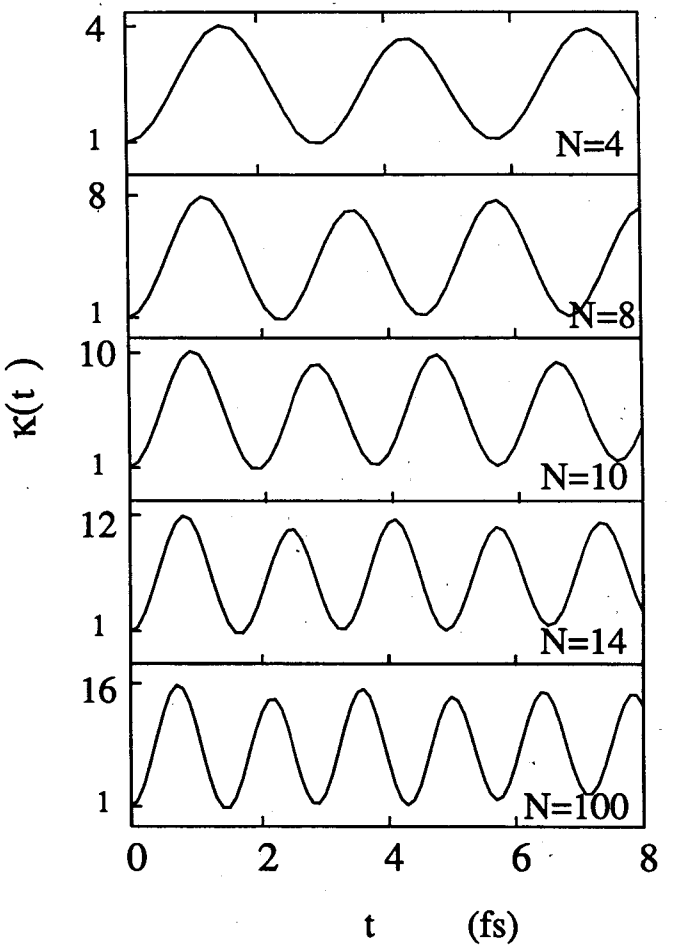

Fig. III.3.10 The inverse participation number $\kappa(t)$ for polyacetylenes with different molecular sizes N in the PPP model.

$N = 100$. In all cases the electron and the hole are created on the same bond so that initially $\kappa(0) \sim 1$ independent on the Coulomb interaction strength. The subsequent evolution is however very different. For the Hückel model ($U = 0$, panel (a)) the pair is uncorrelated and $\kappa(t)$ oscillates between 1 and the polyene size 100. As U is increased in the following panels, the electron and the hole become tightly bound (localized) and the

maximum s values (i.e., exciton delocalization length) decrease. The figure thus clearly illustrates the formation of charge-transfer bound excitons which become more tightly bound as U is increased.

In Fig. III.3.10 we display $\kappa(t)$ for the PPP model for polyacetylene ($U=11.26$ eV) with different sizes ($N=4-100$). From Fig. III.3.9 we know that the exciton coherence size (the amplitude of $\kappa(t)$) is ~ 16 in this case. As long as the molecular size is smaller than the coherence size, the amplitude of $\kappa(t)$ increases with N. The coherence length of the initially prepared doorway state is $\sim N$. As N becomes larger than 16, $\kappa(t)$ does not depend much on N. $\kappa(t)$ for $N=30$ (not shown) is virtually identical to that of $N=100$. The variation of κ with molecular size N is a clear signature of the coherence size of the elementary excitations. These calculations strongly suggest that the variation of $\chi^{(0)}$ with N and U should resemble that of the amplitude κ_m of the inverse participation ratio. Fig. III.3.6 illustrates this point.

In Fig. III.3.11 we display the variation of the static $\chi^{(3)}(0)$ and κ_m with N and U. Fig. III.3.11a demonstrates how the saturation of $\chi^{(3)}(0)$ occurs at smaller N as U increases. In Fig. III.3.11b we display the variation of the amplitude κ_m of the $\kappa(t)$ oscillation with N and U. For the Hückel model ($U=0$) the pair is uncorrelated and κ_m is equal to the polyene size. For the PPP model (as U increased), the electron and the hole become tightly bound and κ_m decreases to 16. We interpret κ_m as the exciton coherence size. As long as the molecular size is larger than the coherence size, the amplitude is unaffected by N. However, as the size decreases further, exciton confinement becomes significant and κ is strongly affected by N. The figure thus clearly illustrates the formation of a charge-transfer bound exciton with delocalization length κ_m which becomes more Frenkel like as U is increased. The variation of the amplitude κ_m with size N and U was shown to be remarkably similar to that of $\chi^{(3)}$, including the sharp nonanalytical behavior of the slope b' ($\kappa_m \sim N^{b'}$) at a critical size $N=18$ [19].

We define the exciton size N_e in the PPP model calculations as the size where the slope of the curves as function of N in Fig. III.3.11b equals one. We have shown [19] that both slopes of κ_m and $\chi^{(3)}(0)$ reach the value of 1 very abruptly in a nonanalytical form (as shown in Fig. III.3.4) and therefore N_c and N_e can be defined unambiguously. The variation of N_c and N_e with molecular size N and the Hubbard interaction U is displayed in Fig. III.3.12. The close correlation between N_c and N_e is a clear signature

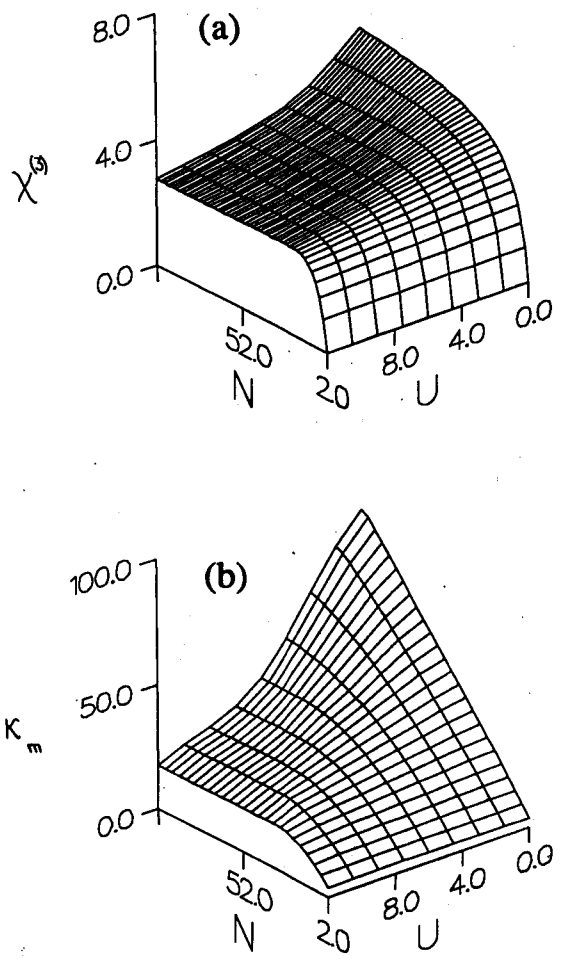

Fig. III.3.11 The variation of the static susceptibility $\chi^{(3)}(0)$ (a) and the amplitude of the inverse participation ratio κ_m (b) for polyacetylene ($\delta=0.07$) with molecular size and Hubbard interaction U.

of the formation of the charge-transfer excitons. Comparing Fig. III.3.12a and III.3.12b shows that the microscopic origin of the large nonlinear optical response and the size saturation of the static susceptibility in conjugated polyenes is related to the dynamics of the relative motion of the charge-transfer excitons.

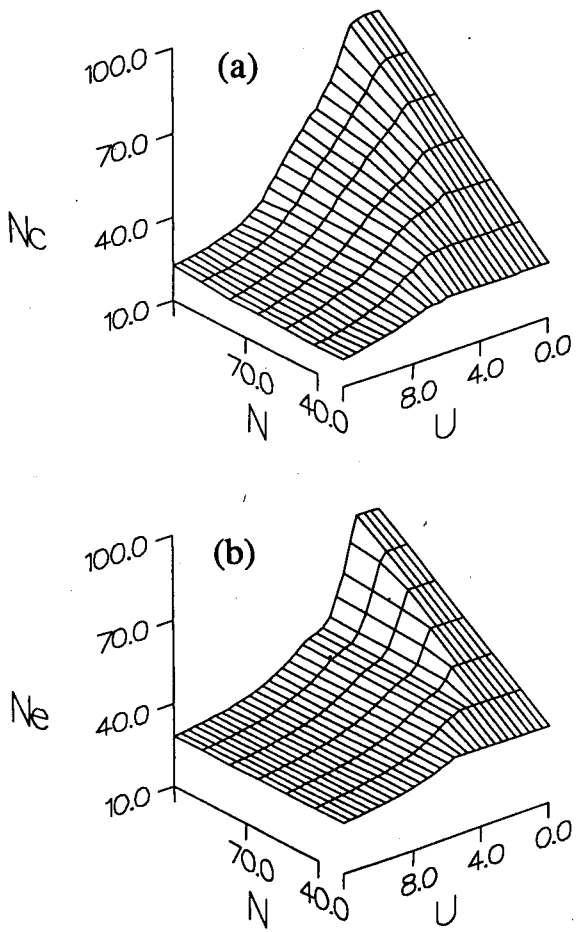

Fig. III.3.12 The variation of the coherence size associated with $\chi^{(3)}(0)$ N_c (a) and that associated with the exciton size N_e (b) for polyacetylene ($\delta = 0.07$) with molecular size and Hubbard interaction U.

III.3.6 Concluding Comments

Our calculations clearly demonstrate the uncorrelated nature of the electron and the hole in the Hückel model, and how the Coulomb attraction of the electron-hole pair changes the nature of the elementary excitations which closely resemble charge-transfer (intermediate) excitons. In addition, the anharmonic oscillator framework provides a real-space picture for the nonlinearity and thus yields a tremendous physical and intuitive insight.

It has been argued that the magnitudes of optical nonlinearities are universal [29c] and that there is no fundamental difference between molecular, semiconductor or conjugated polymer materials. This statement should hold at the single-exciton level, but is clearly an oversimplification, since the nature of higher order dynamical variables (and of the relevant oscillators) are very different for different materials. The differences between various types of materials can be very clearly identified and investigated by analyzing the nature of the anharmonic oscillators in each case using the present picture. These differences are much less transparent when considering the sum-over molecular states expression, which is formally the same for all materials, and whereby the differences enter through interferences among the contributions of the complete set of eigenstates. Conjugated polymer materials can therefore be directly compared with molecular and semiconductor materials. Wannier excitons naturally emerge in the infinite size (continuum) limit.

In our previous studies of Frenkel excitons we found cooperative enhancement associated with the center of mass exciton motion. Simple arguments suggest a possible cooperative enhancement of $\sim N^2$ in $\chi^{(3)}$ of molecular assemblies with Frenkel excitons. This can be rationalized using the molecular eigenstates since the dipole moment scales as $\mu \sim \sqrt{N}$, so that $\chi^{(3)} \sim \mu^4 \sim N^2$. However, an exact cancellation between exciton and two-exciton transitions results in an interference and an overall $\sim N$ scaling for off resonant frequencies [18]. The anharmonic-oscillator picture offers an alternative interpretation of the $\sim N^2$ enhancement and the crossover to $\sim N$ scaling. In accordance with the Pauli exclusion principle, a single site cannot be doubly excited and as a result excitons are not true bosons (or fermions). Linear optical properties can be exactly calculated using the boson approximation for single excitons [13], but the approximation breaks down for the dynamics of two-excitons and higher excitons, which

are vital for the nonlinear optical response and can therefore be probed via second and higher order nonlinear optical techniques. Spatially confining the exciton enhances the nonbosonic nature, and hence the nonlinear susceptibilities (which would vanish if Frenkel excitons were bosons). The combined influence of the Pauli exclusion and excitonic confinement on the third order nonlinear hyperpolarizability results in the cooperative $\sim N^2$ scaling for small sizes and the $\sim N$ scaling for larger sizes where the excitons become more Boson-like. These effects should also show up in the conjugated polyenes through the translational motion of the pair. The incorporation of translational motion in the present theory requires the introduction of additional biexciton variables such as $\langle Y_{sk} Y_{s'k'} \rangle$. In the present treatment we focused primary on the relative motion and factorized these variables. We note a few important differences between the effects of the relative and the translational exciton degree of freedoms on $\chi^{(3)}$. The translational motion gives $b=2$ at most whereas the relative motion gives $b \leq 6$. In addition, the translational enhancement vanishes off-resonance $b=1$ whereas for polyenes it persists also for off-resonance frequencies. The equation of motion approach allows a unified discussion of these effects in both types of materials.

Most practical applications of optical materials use laser frequencies which are far detuned from any molecular resonant frequency (electronic or vibronic). This is done to avoid absorptive losses and other competing processes and to obtain faster switching timescales. The figure of merit for optical materials is defined as the ratio of $\chi^{(3)}$ to the absorption coefficient. Intermolecular (or inter-cell) interactions then do not have enough time to be effective and may be neglected. The optical response of a molecular material thus reduces to essentially that of a single molecule with minor local-field corrections. Spectroscopic applications of nonlinear optics, on the other hand, often use resonant frequencies which provide a direct probe for specific molecular levels and their dynamical behavior. Comparison with resonant spectroscopic measurements should establish the validity of the approximations made in the theory and allow us to predict with confidence the off-resonant optical response. Recent resonant spectroscopic and theoretical studies have suggested the existence of a few "essential" states which dominate the optical response including two-photon resonances in two-photon absorption and third harmonic generation [11]. The present equations of motion automatically focus on the relevant and essential coordinates of the problem and thus provide this picture most naturally.

Finally we note that the recent macroscopic synthesis of C_{60} and C_{70} carbon clusters (buckminsterfullerence) and their derivatives had opened up a new rapidly developing field [34–36]. Nonlinear optical studies have shown that only a few states contribute to the nonlinearity near band gap [35]. Conflicting reports have been made regarding the magnitude of $\chi^{(3)}$. Early studies had reported extremely large $\chi^{(3)}$ whereas more recent studies suggest that C_{60} possesses a nonlinearity comparable to other materials such as polydiacetylenes, ladder polymers and polythiophenes. The present theory is ideally suited for calculating the nonlinear optical response of these interesting materials.

Acknowledgements

The support of the Air Force Office of Scientific Research, the National Science Foundation, and the Center for Photoinduced Charge Transfer, is gratefully acknowledged. We wish to thank Dr. *Brédas* for providing us the numerical values of his calculations of the static $\chi^{(3)}$ and Dr. *S. Etemad* for critical comments.

Appendix: Equations of Motion

In this appendix we present the equations of motion for the dynamical variables $\langle Y_{s,k} \rangle$, $\langle C_{s,k} \rangle$ and $\langle D_{s,k} \rangle$ which are the basis of the theory presented here. In all variables the superscript denotes the order with respect to the field. The equations can be solved successively order by order to yield the optical susceptibilities $\chi^{(1)}$ and $\chi^{(3)}$.

$$-i\hbar \dot{Y}^{(1)}_{s,k} = -\sum_{s'} [\omega^{c}_{s'-s} e^{-ik(s'-s)/2} - \omega^{v}_{s'-s} e^{ik(s'-s)/2} + V_2(s)\delta_{s'+s} - V_1(s)\delta_{s'-s}] Y^{(1)}_{s',k} + E(t)\mu_s \delta_k, \quad \text{(A1a)}$$

$$-i\hbar\dot{Y}^{(2)}_{s,k} = -\sum_{s'}[\omega^{c}_{s'-s}e^{-ik(s'-s)/2} - \omega^{v}_{s'-s}e^{ik(s'-s)/2} + V_2(s)\delta_{s'+s} - V_1(s)\delta_{s'-s}]Y^{(2)}_{s',k} - 2E(t)\sum_{k'}[\mu'_{s'-s}\delta_{k',k} + g_{k-k'}\delta_{s',s}]\sin((ks'-k's)/2)Y^{(1)}_{s',k'}, \quad \text{(A1b)}$$

$$-i\hbar\dot{C}^{(2)}_{s,k} = \sum_{s'}[2\omega^{c}_{s'-s}\sin(k(s'-s)/2) - (V_1(s)-V_1(0))\delta_{s'-s} + \sum_{s''}(V_1(s'')\delta_{s,0} - V_1(s'')\delta_{s',s})]C^{(2)}_{s',k} + E(t)\sum_{s'}[\mu_{s+s'}e^{ik(s+s')/2}Y^{\dagger(1)}_{s',k} - \mu_{s-s'}e^{ik(-s+s')/2}Y^{(1)}_{s',k}], \quad \text{(A1c)}$$

$$-i\hbar\dot{D}^{(2)}_{s,k} = \sum_{s'}[2\omega^{v}_{s'-s}\sin(k(s'-s)/2) - (V_1(s)-V_1(0))\delta_{s'-s} + \sum_{s''}(V_1(s'')\delta_{s,0} - V_1(s'')\delta_{s',s})]D^{(2)}_{s',k} + E(t)\sum_{s'}[\mu_{s-s'}e^{ik(s-s')/2}Y^{\dagger(1)}_{s',k} - \mu_{s-s'}e^{-ik(s+s')/2}Y^{(1)}_{s',k}], \quad \text{(A1d)}$$

$$-i\hbar\dot{Y}^{(3)}_{s,k} = -\sum_{s'}[\omega^{c}_{s'-s}e^{-ik(s'-s)/2} - \omega^{v}_{s'-s}e^{ik(s'-s)/2} + V_2(s)\delta_{s'+s} - V_1(s)\delta_{s'-s}]Y^{(3)}_{s',k} - E(t)\sum_{s'}[\mu_{s'-s}e^{ik(s'-s)/2}C^{(2)}_{s',k} + \mu_{s'+s}e^{ik(s'+s)/2}D^{(2)}_{s',k} - 2E(t)\sum_{k'}[\mu'_{s'-s}\delta_{k',k} + g_{k-k'}\delta_{s',s}]\sin((ks'-k's)/2)Y^{(2)}_{s',k'} - \frac{1}{\sqrt{N}}\sum_{s'k'}[2V_1(s')\sin((k-k')(s'-s/2))(C^{(2)}_{0,k-k'} - D^{(2)}_{0,k-k'})Y^{(1)}_{s,k'} + V_2(s-s')e^{i(k-k')s/2}C^{(2)}_{s'-s,k-k'}Y^{(1)}_{-s'+s,k'} + V_2(s-s'')e^{-i(k-k')s/2}D^{(2)}_{-s'+s,k-k'}Y^{(1)}_{s'-s,k'}], \quad \text{(A1e)}$$

$$-i\hbar\dot{C}^{(3)}_{s,k} = \sum_{s'}[2\omega^{c}_{s'-s}\sin(k(s'-s)/2) - (V_1(s)-V_1(0))\delta_{s'-s} + \sum_{s''}(V_1(s'')\delta_{s,0} - V_1(s'')\delta_{s',s})]C^{(3)}_{s',k} + E(t)\sum_{s'}[\mu_{s+s'}e^{ik(s+s')/2}Y^{\dagger(2)}_{s',k} - \mu_{s-s'}e^{ik(-s+s')/2}Y^{(2)}_{s',k}] - E(t)\sum_{s',k'}2\sin((ks'-k's)/2)[\mu'_{s'-s}\delta_{k,k'} + g_{k-k'}\delta_{s,s'}]C^{(2)}_{s',k}, \quad \text{(A1f)}$$

$$-i\hbar\dot{D}^{(3)}_{s,k}\sum_{s'}[2\omega^{v}_{s'-s}\sin(k(s'-s)/2) - (V_1(s)-V_1(0))\delta_{s'-s} + \sum_{s''}(V_1(s'')\delta_{s,0} - V_1(s'')\delta_{s',s})]D^{(3)}_{s',k} + E(t)\sum_{s'}[\mu_{s-s'}e^{ik(s-s')/2}Y^{\dagger(2)}_{s',k} - \mu_{s+s'}e^{-ik(s+s')/2}Y^{(2)}_{s',k}] + E(t)\sum_{s',k'}2\sin((ks'-k's)/2)[\mu'_{s'-s}\delta_{k,k'} + g_{k-k'}\delta_{s,s'}]D^{(2)}_{s',k}. \quad \text{(A1g)}$$

The equation for $Y^{\dagger}_{s,k}$ is the hermitian conjugate of Eq. (A1e). ω^{c}_{s} and ω^{v}_{s} are defined as

$$\omega^{c}_{s} = \pm\beta/\sqrt{2}\sum_{k}e^{-iks}\varepsilon_{ck} + \delta_{s,0}\sum_{s'}[V_1(s') - V_2(0)], \quad \text{(A2)}$$

$$\omega^{v}_{s} = \pm\beta/\sqrt{2}\sum_{k}e^{-iks}\varepsilon_{vk} + \delta_{s,0}\sum_{s'}[V_1(0) - V_1(s')]. \quad \text{(A3)}$$

The variation of μ, ω, V_1, V_2 with s was calculated earlier [19].

References

[1] *D. J. Williams* (ed.), Nonlinear Optical Properties of Polyatomic Materials, ACS Ser. 233. American Chemical Society, Washington, D.C. 1985.

[2] *H. Kuzang, M. Mehing,* and *S. Roth* (eds.), Electron Properties of Polymers and Related Compounds, Springer Ser., Solid State Sci., 63. Springer-Verlag, Berlin 1985.

[3] *D. S. Chemla* and *J. Zyss*, Nonlinear Optical Properties of Organic Molecules and Crystals, Vols. 1 and 2. Academic, Orlando 1987.
[4] (a) *S. Etemad* and *Z. G. Soos*, in: Spectroscopy of Advanced Materials, ed. by *R. J. H. Clark* and *R. E. Hester*. Wiley, New York 1991; (b) *Z. G. Soos*, in: Electroresponsive and Polymeric Systems, Vol. 1, ed. by *T. A. Marcel*. Dekker, New York 1988.
[5] (a) *S. N. Dixit, D. D. Guo*, and *S. Mazumdar*, Mol. Cryst. Liq. Cryst. **194** (1991) 33; (b) *S. Mazumdar* and *S. N. Dixit*, Synth. Met. **28** (1989) D463; (c) *S. Mazumdar* and *D. K. Campbell*, Phys. Rev. Lett. **55** (1985) 2067.
[6] *A. F. Garito, J. R. Heflin, F. Y. Wong*, and *Q. Zamani-Khamiri*, in: Organic Materials for Nonlinear Optics, ed. by *R. A. Hann* and *D. Bloor*. Special Publication No. 69, Royal Soc. of Chem., London 1988; *J. R. Heflin, K. Y. Wong, Q. Zamani-Khamiri*, and *A. F. Garito*, Phys. Rev. **B38** (1988) 157; Mol. Crys. Liq. Crys. **160** (1988) 37.
[7] *C. P. deMelo* and *R. Silbey*, Chem. Phys. Lett. **140** (1987) 531; J. Chem. Phys. **88** (1988) 2563.
[8] *J. Zyss*, J. Chem. Phys. **70** (1979) 3333.
[9] *E. F. McIntyre* and *H. F. Hameka*, J. Chem. Phys. **68** (1978) 3481.
[10] (a) *Z. Shuai* and *J. L. Brédas*, Phys. Rev. **B44** (1991) 5962; (b) *D. N. Beratan, J. N. Onuchic*, and *J. W. Perry*, J. Phys. Chem. **91** (1987) 2696.
[11] (a) *B. S. Hudson* and *B. E. Kohler*, Chem. Phys. Lett. **14** (1972) 299; (b) *B. S. Hudson* and *B. E. Kohler*, J. Chem. Phys. **59** (1973) 4984; (c) *B. S. Hudson, B. E. Kohler*, and *K. Schulten*, Excited States **6** (1982) 1; *B. E. Kohler*, J. Chem. Phys. **93** (1990) 5838.
[12] *S. Schmitt-Rink, D. S. Chemla*, and *D. A. B. Miller*, Phys. Rev. **B32** (1985) 6601; *S. Schmitt-Rink, D. A. B. Miller*, and *D. S. Chemla*, Phys. Rev. **B35** (1987) 8113; *S. Schmitt-Rink, D. S. Chemla*, and *D. A. B. Miller*, Adv. in Phys. **38** (1989) 89.
[13] *A. Stahl* and *D. Baslev*, Electrodynamics of the Semiconductor Band Edge, Springer-Verlag, Berlin 1987.
[14] (a) *Z. G. Soos* and *S. Ramasheba*, J. Chem. Phys. **90** (1989) 1067; (b) *Z. G. Soos* and *S. Ramasheba*, Phys. Rev. **B29** (1984) 5410.
[15] *W.-S. Fann, S. Benson, J. M. Madey, S. Etemad, G. L. Baker*, and *F. Kajdar*, Phys. Rev. Lett. **62** (1989) 1492; *P. D. Townsend, W.-S. Fann, S. Etemad, G. L. Baker, Z. G. Soos*, and *P. C. M. McWilliams*, Chem. Phys. Lett. **180** (1991) 485.
[16] *J. Yu, B. Friedman, P. R. Baldwin*, and *W. P. Su*, Phys. Rev. **B39** (1989) 12814; *W. P. Su, J. R. Schrieffer*, and *A. J. Heeger*, Phys. Rev. **B22** (1980) 2099; *S. Abe* and *W. P. Su*, Mol. Cryst. Liq. Cryst. **194** (1991) 357.
[17] *C.-Q. Wu* and *X. Sun*, Phys. Rev. **B42** (1990) 9736; *W. Wu*, Phys. Rev. Lett. **61** (1988) 1119; *W. K. Wu* and *S. Kivelson*, Synth. Met. **28** (1989) D575.
[18] *F. C. Spano* and *S. Mukamel*, Phys. Rev. **A40** (1989) 5783; *O. Dubovsky* and *S. Mukamel*, J. Chem. Phys. **96** (1992) 9201; *S. Mukamel*, in: Nonlinear Optical Properties of Organic Molecules and Crystals, Vol. 3, ed. by *J. Zyss*. Academic, New York, 1993; *J. A. Leegwater* and *S. Mukamel*, Phys. Rev. **A46** (1992) 452.
[19] *H. X. Wang* and *S. Mukamel*, Chem. Phys. Lett. **192** (1992) 417; *S. Mukamel* and *H. X. Wang*, Phys. Rev. Lett. **69** (1992) 65; J. Chem. Phys. **97** (1992) 8019.
[20] *F. F. So, S. R. Forrest, Y. Q. Shi*, and *W. H. Steier*, Appl. Phys. Lett. **56** (1990) 674; *D. Mobius* and *H. Kuhn*, Isr. J. Chem. **18** (1979) 375 J. Appl. Phys. **64** (1988) 5138; Langmuir-Blodgett Films, ed. by *G. Roberts*. Plenum, New York 1990; *M. G. Bawendi, M. L. Steigerwald*, and *L. E. Brus*, Ann. Rev. Phys. Chem. **41** (1990) 477; *Y. Wang*, J. Opt. Soc. Am. **B8** (1991) 981.
[21] (a) *J. P. Hermann* and *J. Ducuing*, J. Appl. Phys. **45** (1974) 5100; (b) *K. C. Rustagi* and *J. Ducuing*, Optics Communications **10** (1974) 258.
[22] *G. P. Agrawal, C. Cojan*, and *C. Flytzanis*, Phys. Rev. **B17** (1978) 776; *C. Flytzanis*, in: Nonlinear Optical Properties of Organic Molecules and Crystals, Vol. 2, ed. by *D. S. Chemla* and *J. Zyss*. Academic, Orlando 1987, p. 121.
[23] *J. R. Kuklinski* and *S. Mukamel*, Phys. Rev. **B42** (1990) 295; Chem. Phys. Lett. **189** (1992) 119.
[24] *L. Salem*, The Molecular Orbital Theory of Conjugated System. W. A. Benjamin, New York 1966.
[25] *N. Bloembergen*, Nonlinear Optics, W. A. Benjamin, New York 1965.
[26] (a) *F. C. Spano* and *S. Mukamel*, Phys. Rev. Lett. **66** (1991) 1197; (b) *O. Dubovsky* and *S. Mukamel*, J. Chem. Phys. **95** (1991) 7828.
[27] *J. Knoester* and *S. Mukamel*, Phys. Rep. **205** (1991) 1.
[28] *S. Mukamel*, Adv. Chem. Phys. **70** (1988) 165.
[29] (a) *S. Suhai*, J. Chem. Phys. **85** (1986) 611; (b) *B. I. Greene, J. Orenstein, R. R. Millard*, and *L. R. Williams*, Phys. Rev. Lett. **58** (1987) 2750; (c) *B. I. Greene, J. Orenstein*, and *S. Schmitt-Rink*, Science **247** (1990) 679.
[30] *F. Kajzar, L. Rothberg, S. Etemad, P. A. Chollet, D. Grec, A. Boudet*, and *T. Jedju*, Thin Sol. Films **160** (1988) 1.
[31] *M. Pope* and *C. Swenberg*, Electronic Processes in Organic Crystals. Clarence Press, New York 1982.
[32] *V. M. Agranovich* and *M. D. Galanin*, Electronic Exciton Energy Transfer in Condensed Matter. North-Holland, Amsterdam 1982.
[33] *E. N. Economou*, Green's Functions in Quantum Physics. Springer-Verlag, Berlin 1983.
[34] *W. Kratschmer, L. D. Lamb, K. Fostiropoulos*, and *D. R. Huffman*, Nature **347** (1990) 354.
[35] *Y. Wang* and *L.-T. Cheng*, submitted for publication; *J. S. Meth, H. Vanherzeele*, and *Y. Wang*, Phys. Rev. Lett., submitted; *Y. Wang* and *L.-T. Cheng*, presented at: Workshop on Fullerities and Solid States Derivatives, University of Pennsylvania, Aug. 2–3, 1991.
[36] *W. J. Blau, H. J. Byrne, D. J. Cardin, T. J. Dennis, J. P. Hare, H. W. Kuoto, R. Taylor*, and *D. R. M. Walton*, Phys. Rev. Lett. **67** (1991) 1423.